Solid-State Electronics 79 (2013) 274–280

Contents lists available at SciVerse ScienceDirect

Solid-State Electronics

journal homepage: www.elsevier.com/locate/sse

Enhanced hole mobility and density in GaSb quantum wells

Brian R. Bennett *, Theresa F. Chick, Mario G. Ancona, J. Brad Boos

Electronic Science and Technology Division, Naval Research Laboratory, Washington, DC 20375, United States

ARTICLE INFO

Article history:
Received 17 May 2012
Received in revised form 16 July 2012
Accepted 22 August 2012
Available online 8 October 2012

The review of this paper was arranged by Prof. E. Calleja

Keywords:
Molecular beam epitaxy
Quantum wells
Semiconducting III–V materials
Field-effect transistors
GaSb

ABSTRACT

Modulation-doped quantum wells (QWs) of GaSb clad by AlAsSb were grown by molecular beam epitaxy on InP substrates. By virtue of quantum confinement and compressive strain of the GaSb, the heavy- and light-hole valence bands in the well are split and the hole mobility is thereby significantly enhanced. Room-temperature Hall mobilities as high as 1200–1500 $cm^2/V\,s$ were achieved for 5–10 nm QWs and biaxial strains of 1–3%. This contrasts with earlier work on GaSb/AlGaAsSb QWs on GaAs substrates in which the mobilities were found to fall off above 1% strain. Moreover, unlike in comparable InGaSb and InSb QWs, the high mobilities were maintained out to sheet densities of $3.5 \times 10^{12}/cm^2$. As a result, the sheet resistivities observed in the GaSb/AlAsSb wells reached record levels as low as 1500 Ω/□. Modeling indicates that this performance gain is due to the larger valence band offset of the GaSb QWs and the consequent reduction in scattering because of the better confinement and the lower doping levels needed for a given sheet charge.

Published by Elsevier Ltd.

1. Introduction

Narrow bandgap compound semiconductors exhibit high electron mobilities and peak velocities. The high velocities are reached at relatively low electric fields, enabling analog electronic devices with extremely low power consumption. For example, low-noise amplifiers (LNAs) using high-electron-mobility transistors (HEMTs) with InAs channels and AlSb barriers operate at substantially lower power than similar circuits based upon GaAs or Si [1]. Recently, there has been interest in the potential of III–V transistors for advanced logic applications which could enhance digital circuit functionality and extend Moore's law [2]. For these applications, a key to low power operation is the ability to make complementary circuits. In III–V materials, one challenge centers on maximizing the hole mobility in p-channel field-effect transistors (FETs) [3–5].

Like in Si and Ge, the hole mobilities of III–V compounds are generally low and, for this reason, researchers have exploited quantum confinement and strain as a means of splitting the heavy-hole and light-hole valence bands and giving lower in-plane hole masses and enhanced low-field mobility [3–14]. The antimonides offer the highest hole mobilities of the III–V compounds, with room-temperature values approaching 1000 $cm^2/V\,s$ for bulk GaSb and InSb. We previously demonstrated compressively-strained high-mobility p-type InGaSb QWs confined by AlGaSb barriers layers [7]. In this work, we investigate compressively-strained GaSb QWs confined by AlAsSb barrier layers [6,11,15]. Compared to the InGaSb QW, the GaSb QW has a larger valence band offset and bandgap, and may also be advantageous in being a binary and so not subject to alloy scattering in the well. The structures are grown on metamorphic AlAsSb buffer layers on InP substrates. This combination is found to yield room-temperature mobilities as high as 1500 $cm^2/V\,s$ and sheet resistivities as low as 1500 Ω/□, with the latter value a factor of two lower than the best previously achieved for III–V p-type quantum wells.

2. Experimental procedures

The heterostructures studied here are grown by molecular beam epitaxy (MBE) on semi-insulating (001) InP substrates using a Riber Compact 21T MBE system. A cross-section is shown in Fig. 1a. The first layer is 160 nm of $In_{0.52}Al_{0.48}As$ lattice matched to InP, followed by a ~1.3 μm buffer layer of $AlAs_xSb_{1-x}$, an optional 4 nm Be-doped $AlAs_xSb_{1-x}$ donor layer, a 9.5 nm $AlAs_xSb_{1-x}$ spacer, a 5–10 nm GaSb QW, a 10.5 nm $AlAs_xSb_{1-x}$ barrier, a 4 nm $In_{0.2}Al_{0.8}Sb$ etch-stop, and a 2 nm InAs cap. The $AlAs_xSb_{1-x}$ layers were grown as a digital alloy by toggling the As and Sb shutters while the Al shutter and the As and Sb valves remained open, allowing better control of composition compared to random alloys [16,17]. The AlAs mole fraction was adjusted by changing the length of time the As shutter is open relative to the Sb shutter. As shown in the calculated band-structure, Fig. 1b, there is a large valence band discontinuity between the AlAsSb and the GaSb, providing for good confinement of holes in the GaSb. The $AlAs_xSb_{1-x}$ is almost fully relaxed; its composition dictates the amount of biaxial

* Corresponding author.
E-mail address: brian.bennett@nrl.navy.mil (B.R. Bennett).

0038-1101/$ - see front matter Published by Elsevier Ltd.
http://dx.doi.org/10.1016/j.sse.2012.08.004

Report Documentation Page

Form Approved
OMB No. 0704-0188

1. REPORT DATE	2. REPORT TYPE	3. DATES COVERED
OCT 2013		**00-00-2013 to 00-00-2013**

4. TITLE AND SUBTITLE	5a. CONTRACT NUMBER
Enhanced hole mobility and density in GaSb quantum wells	5b. GRANT NUMBER
	5c. PROGRAM ELEMENT NUMBER
6. AUTHOR(S)	5d. PROJECT NUMBER
	5e. TASK NUMBER
	5f. WORK UNIT NUMBER
7. PERFORMING ORGANIZATION NAME(S) AND ADDRESS(ES) **Naval Research Laboratory,Electronic Science and Technology Division,Washington,DC,20375**	8. PERFORMING ORGANIZATION REPORT NUMBER
9. SPONSORING/MONITORING AGENCY NAME(S) AND ADDRESS(ES)	10. SPONSOR/MONITOR'S ACRONYM(S)
	11. SPONSOR/MONITOR'S REPORT NUMBER(S)

12. DISTRIBUTION/AVAILABILITY STATEMENT
Approved for public release; distribution unlimited

13. SUPPLEMENTARY NOTES

14. ABSTRACT

Modulation-doped quantum wells (QWs) of GaSb clad by AlAsSb were grown by molecular beam epitaxy on InP substrates. By virtue of quantum confinement and compressive strain of the GaSb, the heavy- and light-hole valence bands in the well are split and the hole mobility is thereby significantly enhanced. Room-temperature Hall mobilities as high as 1200?1500 cm2/V s were achieved for 5?10 nm QWs and biaxial strains of 1?3%. This contrasts with earlier work on GaSb/AlGaAsSb QWs on GaAs substrates in which the mobilities were found to fall off above 1% strain. Moreover, unlike in comparable InGaSb and InSb QWs, the high mobilities were maintained out to sheet densities of 3.5 1012/cm2. As a result the sheet resistivities observed in the GaSb/AlAsSb wells reached record levels as low as 1500 X/h. Modeling indicates that this performance gain is due to the larger valence band offset of the GaSb QWs and the consequent reduction in scattering because of the better confinement and the lower doping levels needed for a given sheet charge.

15. SUBJECT TERMS

16. SECURITY CLASSIFICATION OF:			17. LIMITATION OF ABSTRACT	18. NUMBER OF PAGES	19a. NAME OF RESPONSIBLE PERSON
a. REPORT **unclassified**	b. ABSTRACT **unclassified**	c. THIS PAGE **unclassified**	**Same as Report (SAR)**	**7**	

InAs	2 nm
$In_{0.2}Al_{0.8}Sb$	4 nm
$AlAs_xSb_{1-x}$	10.5 nm
GaSb	5-10 nm
$AlAs_xSb_{1-x}$	9.5 nm
$AlAs_xSb_{1-x}$(Be)	4 nm
$AlAs_xSb_{1-x}$	1.3 μm
$In_{0.52}Al_{0.48}As$	0.16 μm
SI InP (001)	substrate

(a)

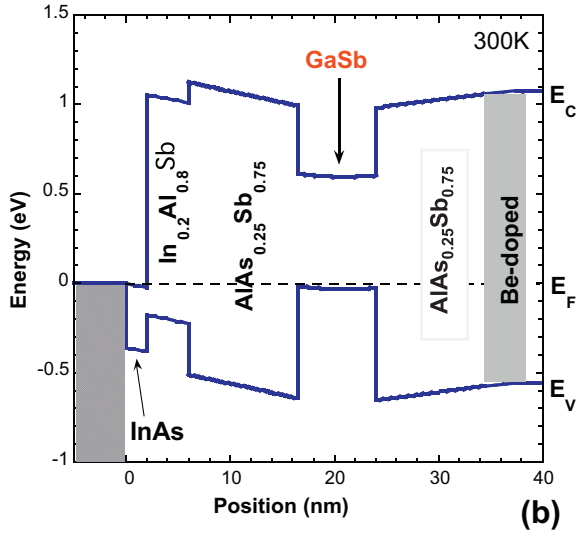

Fig. 1. (a) Cross-section of GaSb/AlAsSb QW heterostructures. The $AlAs_xSb_{1-x}$ layers are composed of AlSb/AlAs short-period superlattices. (b) Calculated band-structure for a GaSb/$AlAs_{0.25}Sb_{0.75}$ QW with a hole sheet density of $1.0 \times 10^{12}/cm^2$.

strain in the GaSb QW. For a buffer layer of $AlAs_xSb_{1-x}$, the in-plane biaxial strain associated with the lattice mismatch between the well and buffer layer is given by:

$$\varepsilon = \frac{6.0954}{6.1355 - 0.4736x} - 1 \quad (1)$$

The MBE growth temperature is near 450 °C for the InAlAs. The temperature is then raised to 520 °C for the $AlAs_xSb_{1-x}$ buffer layer, and then reduced back to 450 °C for the GaSb QW and subsequent layers. The GaSb QW and InAs cap were grown at a rate of 0.2 monolayers (ML)/s, and other layers were grown near 1.0 ML/s as calibrated from reflection high-energy electron diffraction oscillations.

Based upon previous results on this MBE system, we expect the layer thicknesses to be uniform to within 1% across the 76-mm-diameter substrate if the wafer is rotated. Table 1 includes relevant parameters for the nine MBE growths in this study. For six growths (#1–5 and 8), the wafers were rotated during all the layers except the $AlAs_xSb_{1-x}$ buffer layer. This resulted in AlAs mole fractions (and hence GaSb strain) which varied by more than a factor of two across the wafer. Several 5 × 5 mm squares were then cleaved from different locations on each wafer to provide a range of samples with varying strain in a highly efficient manner. For three

Table 1
Growth parameters for the samples in this study. Resistivity values are from contactless wafer mapping, and are not well-calibrated above 15,000 Ω/□.

Growth#	QW thickness (nm)	Dopant	Substrate	Rotate-buffer	Rotate-doping	Resistivity Ω/□
1	10	None	InP	N	Y	7100–18,000
2	7.5	None	InP	N	Y	7700–17,000
3	5	None	InP	N	Y	6500–27,000
4	7.5	Be	InP	N	Y	2100–4200
5	7.5	Be	GaAs	N	Y	2400–6700
6	7.5	Be	InP	Y	N	2200–4500
7	7.5	Be + Be	InP	Y	N	1800–3900
8	7.5	Si	InP	N	Y	4100–>50,000
9	7.5	Si	InP	Y	N	10,000–>50,000

growths (#6, 7, and 9), the wafers were rotated for all layers except the 4 nm layer(s) of $AlAs_xSb_{1-x}$ doped with Be or Si. This resulted in a gradient in the dopant concentration and hence hole sheet density across the wafers.

Hall/van der Pauw transport measurements were performed on a total of 79 samples at 300 K, using magnetic fields of 0.37, 0.55 and 1.0 T. Measurements were performed at two or more current levels at each B field, and average values are given in this paper with standard deviations usually less than 5%. Room-temperature, 55-point resistivity maps were generated for each wafer from eddy-current measurements using a contactless Lehighton 1500 system [18]. Atomic force microscopy (AFM) measurements were performed on selected samples to yield root-mean-square (rms) roughness over 5 × 5 μm regions. X-ray diffraction (XRD) measurements were made on a double-crystal system using Cu-Kα radiation and compared to simulations using dynamical diffraction theory.

3. Results and discussion

In Fig. 2, we show the resistivity map for growth #4, a Be-doped sample with a 7.5 nm GaSb QW, grown on an InP substrate. The resistivity varied from 2060 to 4240 Ω/□. A 5-mm wide strip was cleaved as indicated, yielding twelve 5 × 5 mm samples for characterization. The transport results will be discussed later.

AFM data was collected on several samples with a variety of strains and hole densities. The rms roughness was between 0.5 and 1.0 nm, with no clear correlation to mobility or other parameters (substrate, QW thickness, doping). These values are as good or better than what was measured for InAs-channel HEMT structures on Al(Ga)Sb buffer layers and GaAs or InP substrates and are fully compatible with monolithic-microwave integrated circuit (MMIC) processing [19,20].

In Fig. 3, we show the XRD scan for sample 4L, the piece labeled L in Fig. 2. The buffer layer consisted of 888 periods of (4.0 s AlSb/1.0 s AlAs). Peaks are visible for the InP substrate and the short-period superlattice ($n = -2$, -1, 0, and +1). A simulation was generated by adjusting the superlattice thicknesses to match the experimental peak positions, and is shown below the experimental data in Fig. 3. The layer thicknesses were 0.33 nm AlAs and 1.30 nm AlSb, yielding a period of 1.63 nm. The lattice relaxation for the superlattice was assumed to be 100%. Based upon the nominal

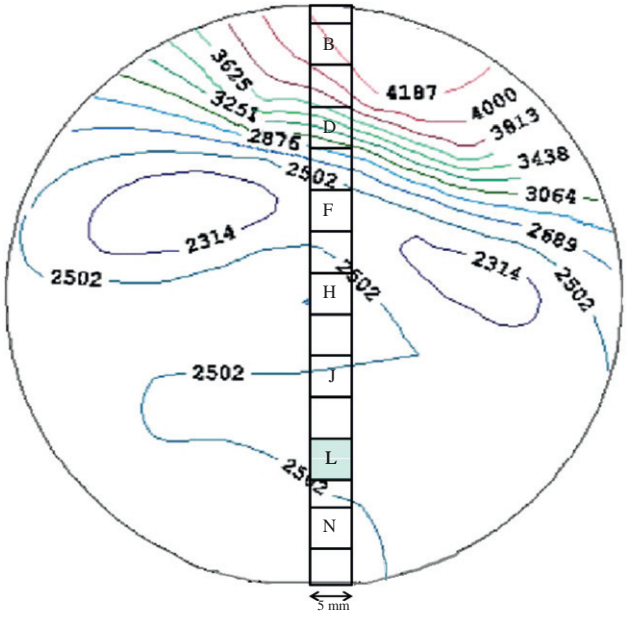

Fig. 2. Resistivity map in units of Ω/sq for growth #4. The gradient across the 76-mm wafer is a result of varying strain and mobility in the GaSb QW.

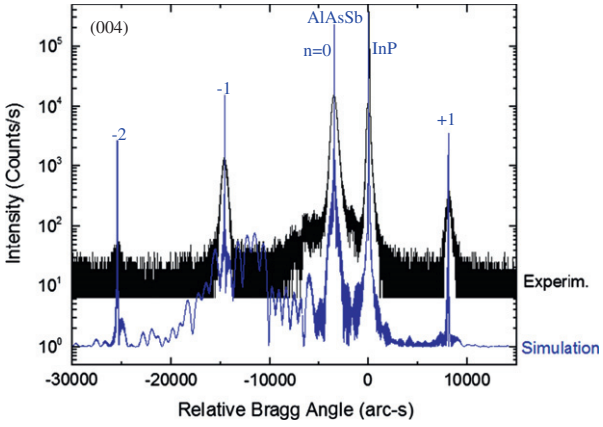

Fig. 3. Double-crystal X-ray diffraction data for sample 4L (upper curve) and simulation (lower curve). AlSb and AlAs thicknesses in the buffer layer short-period superlattice were varied to obtain a good fit to the experimental data.

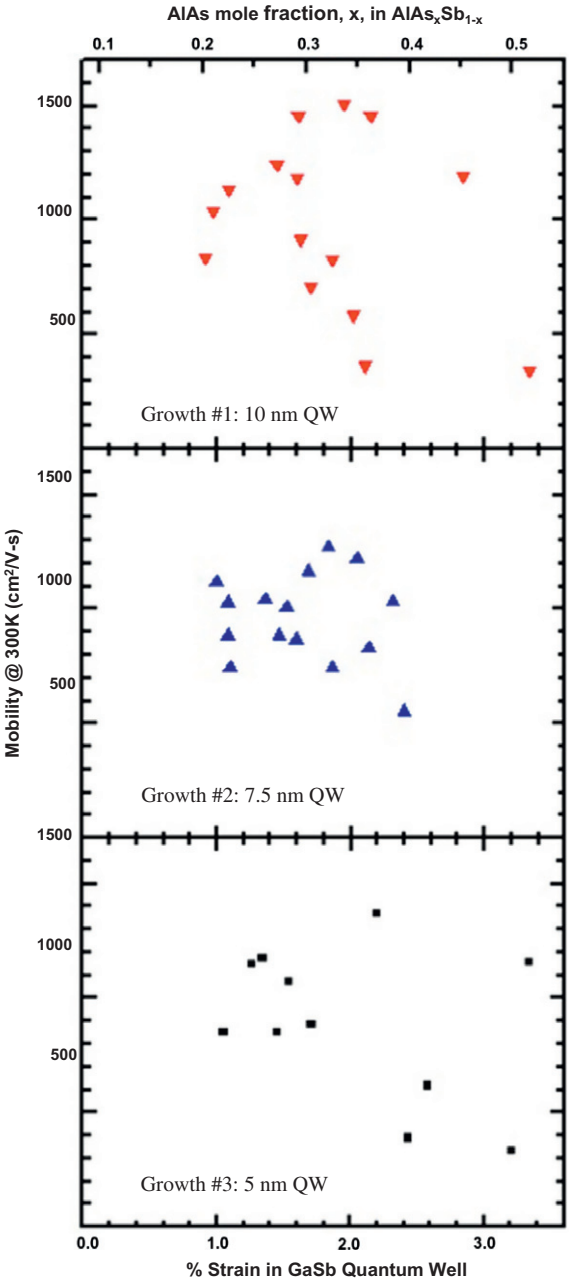

Fig. 4. Room-temperature mobility as a function of GaSb QW strain (or buffer layer composition) for growths #1–3, differing only in QW thickness. The samples were not intentionally doped.

growth rates, we expect a period of 1.50 nm in the center of wafer #4; L is in a region of higher Al flux than the center. The buffer layer thickness is 1.45 μm (888 × 1.63 nm). The epilayer peaks are all broadened compared to the simulation. For example, the full-width at half-maximum for the $n = 0$ superlattice peak is 520 arc-s. This is a result of a high density of misfit dislocations required to relax the lattice mismatch. Using the superlattice layer thicknesses and Vegard's law, we calculate the effective ternary composition to be $AlAs_{0.202}Sb_{0.798}$. Using Eq. (1), the compressive biaxial strain in the GaSb is 0.92%. Samples with higher AlAs mole fractions generally exhibited weaker satellite peaks. This indicates that the superlattices are not as well defined but does not imply lower crystalline quality.

MBE growths #1–3 did not include a doping layer. The growths were nominally identical except for the thickness of the channel layer. There was no rotation during the growth of the AlAsSb buffer layer. All the samples from these three growths were p-type, with hole sheet concentrations of $1.0 \pm 0.3 \times 10^{12}$ cm^{-2}; these results are consistent with previous results for undoped GaSb and InGaSb quantum wells (QWs) [6,7,9]. In Fig. 4, we plot the measured room-temperature mobility as a function of strain for (a) growth #1, 10 nm QW, (b) growth #2, 7.5 nm QW, and (c) growth #3, 5 nm QW. For each growth, we observe considerable strain-induced mobility enhancement compared to unstrained GaSb QWs (μ = 200–400 cm^2/V s, see Refs. [6,21,22]). For growth #1, we observe an increase in mobility as strain increases from 1.0 to 1.5%. For higher strains, there are substantial variations in the mobility. One sample with a strain of 2.0% has a mobility of 1500 cm^2/V s. This is a record value for GaSb and matches the highest values for InGaSb [7]–the largest of any III–V material at room temperature. The three samples with mobilities of 1400–1500 cm^2/V s and strains of 1.6–2.1% were adjacent to one another on the wafer. The four samples in the same strain range and mobilities of

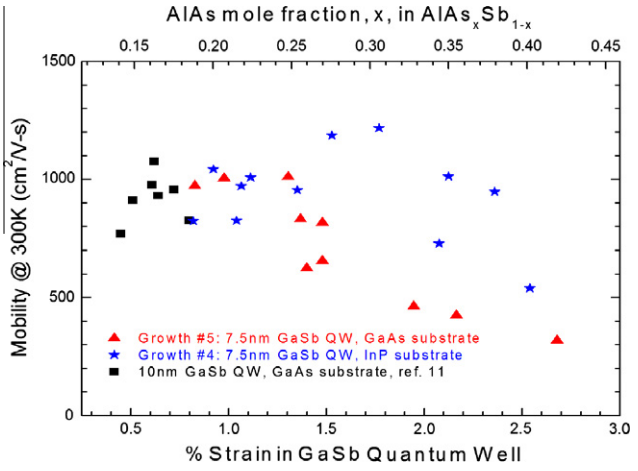

Fig. 5. Room-temperature mobility as a function of GaSb QW strain (or buffer layer composition) for samples with Be modulation doping. Note the difference between InP and GaAs substrates.

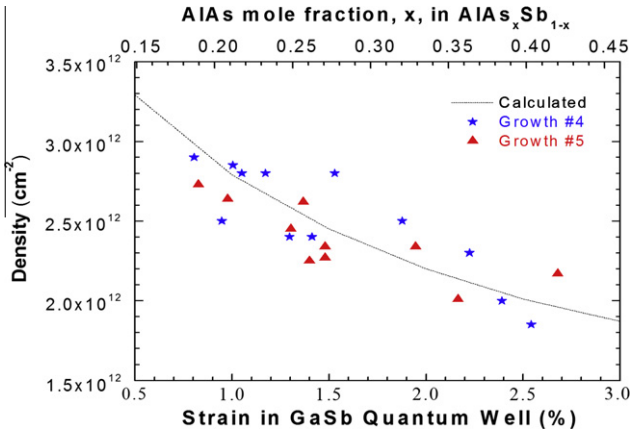

Fig. 6. Channel density as a function of QW strain for samples from wafers #4 and 5. Solid line represents calculated values.

400–800 cm^2/V s were from a different area of the wafer. Similar trends were observed for growths #2 and 3. This suggests that one or more parameters other than strain are important. Possibilities include buffer layer growth rate and thickness, V:III flux ratios, and growth temperature. The XRD measurements allowed us to determine the buffer layer growth rate and thickness for each sample. There was not a clear correlation with mobility. We expect significant variations in flux ratios and substrate temperature across the wafer during the buffer layer growth when it is not rotating, but cannot measure these values across the wafer. There is an apparent correlation between the sheet density and mobility for samples with strain near 2% on all three growths, with the high-mobility samples having densities about 20% lower than the low-mobility samples. Although higher density could cause lower mobility, it seems much more likely that the two effects arise from a common underlying mechanism (e.g. defects). Given the fact that high-mobility samples were found for each of the three growths for strains near 2%, we expect that if this strain regime were targeted and growths were performed with substrate rotation throughout, one could identify growth conditions that ensure consistently high mobilities.

Growth #4 was identical to #2 (7.5 nm QW) except that Be doping was added to achieve higher sheet concentrations. The results are plotted as stars in Fig. 5. The average sheet density was $2.5 \times 10^{12}\ cm^{-2}$, with the particular values clearly correlating with strain and ranging from $2.9 \times 10^{12}\ cm^{-2}$ for 0.8% strain to $1.9 \times 10^{12}\ cm^{-2}$ for 2.5% strain. The transport data is consistent with the resistivity data in Fig. 2. It is important to point out that the results for growths #1–4 contrast with earlier work from our group as well as that of Tokranov et al. [11] in not showing a consistent degradation in GaSb mobility for higher strains. Our earlier work [6] (not shown here for clarity) found a drop above ~1% strain, while Tokranov observed the mobility to peak at about 0.6% strain as shown in Fig. 5. A possible explanation for this discrepancy is that both sets of earlier studies used GaAs substrates, whereas the new experiments used InP substrates. To confirm this, we grew a wafer (#5) identical to #4 except that the substrate was GaAs and the InAlAs buffer layer was replaced by epitaxial GaAs. The results, plotted as triangles in Fig. 5, show decreasing mobility for strains above 1.3% in rough agreement with the earlier experiments.

To aid in understanding the results of this paper, we have performed a set of 8 × 8 k.p calculations using the nextnano program [23]. We used the heterostructure shown in Fig. 1 with a 7.5 nm QW to match growths #4 and 5. The background density was set at $7 \times 10^{11}\ cm^{-2}$ and the Be dopant concentration was adjusted to yield $2.2 \times 10^{12}\ cm^{-2}$ at a 2% compressive strain for the GaSb. In Fig. 6, we plot the channel density as a function of QW strain. We also include the data points from wafers #4 and #5. The good agreement between the calculated and experimental data indicates that the drop in density is due to a reduced transfer of charge from the doped layer caused by the rise in the (hole) energy of the valence band states in the QW induced by the increasing compressive strain. This agreement also suggests that we understand our system both from experimental and theoretical viewpoints. With respect to the former, it is interesting to note that it was the use of multiple samples from a single MBE growth that made this comparison possible. Had these been separate growths, the unintentional day-to-day variations in MBE conditions would have made it difficult to observe such small density changes.

The poorer quality GaSb seen at high strains when on a GaAs as opposed to an InP substrate could certainly result from the former substrate having a higher defect density. However, the fact that high mobilities were previously obtained for strains up to 2% for InGaSb [7] and InSb QWs[10] despite using GaAs substrates suggests that the trouble is not with the substrate per se. Instead we speculate that the substrate dependence for GaSb QWs arises from defects in the AlAsSb buffer layer. For layers above the thermodynamic critical layer thickness, the degree of lattice relaxation may depend on the particular defects in the layer on which the strained layer is grown [24–26]. If there is a higher density (or a different type) of dislocations for AlAsSb on GaAs compared to AlAsSb on InP, then the GaSb films could relax more in the former case for equivalent strains. In the simplest case, if the misfit dislocation types were the same for fully relaxed AlAsSb buffer layers grown on InP and GaAs, then the layers grown on GaAs would have a factor of two higher misfit dislocation density, reflecting the factor of two larger mismatch between the buffer layer and substrate. This could lead to a peak in mobility at lower strains for growth on GaAs. In the case of InSb and InGaSb QWs, their use of different buffers layers (InAlSb and AlGaSb, respectively) means their dependence on the substrate can be entirely different.

In Fig. 7, we plot hole mobility as a function of sheet concentration for InSb [10] and InGaSb [7] QWs. The hole mobilities for both channel materials decrease as carrier density increases. To explore this relationship for GaSb/AlAsSb/InP heterostructures, we grew two wafers, #6 and #7, in which the samples were rotated during all layers except the AlAsSb(Be) doping layer(s). As discussed earlier, this should yield a gradient in Be concentration across the wafer and hence allow a range of hole densities to be investigated

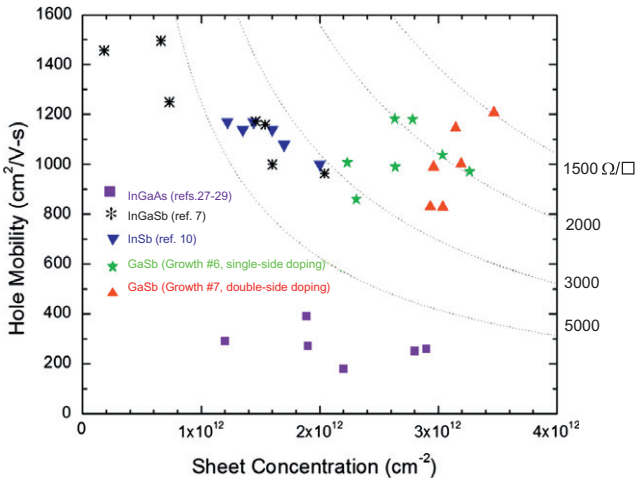

Fig. 7. Room-temperature hole mobility as a function of sheet concentration for growths #6 and 7 as well as data from the literature for InGaSb, InSb, and InGaAs.

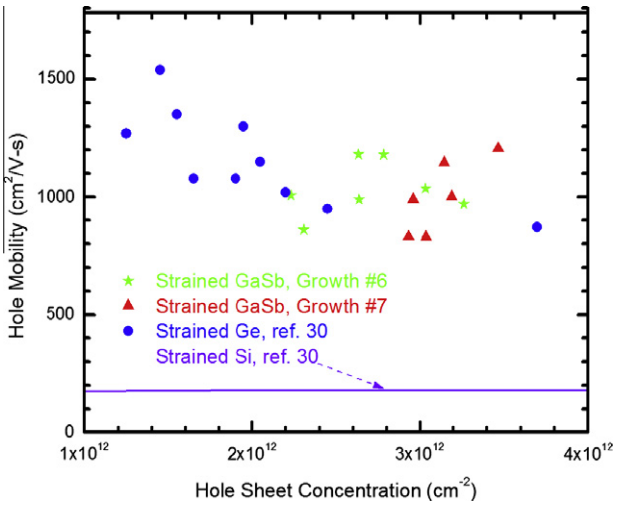

Fig. 8. Room-temperature hole mobility as a function of sheet concentration for growths #6 and 7 as well as data from the literature for strained Ge and strained Si.

with a single growth. A buffer layer composition of $AlAs_{0.29}Sb_{0.71}$, corresponding to a GaSb strain of 1.7% was chosen. The GaSb thickness was 7.5 nm. The Be cell temperature (879 °C) was the same as in wafers #4 and #5. The data for wafer #6, with single-sided Be doping as shown in Fig. 1, are plotted as stars in Fig. 7. The sheet densities vary by a factor of 1.5 across the wafer. Wafer #7 had double-side doping, with 4 nm layers of AlAsSb(Be) on both sides of the QW and 5.4 nm spacer layers. The Be temperature was again 879 °C. The results, shown as up-triangles in Fig. 7, show less variation in density across the wafer than for #6. Simulations discussed below show that this is likely due to a saturation in the ability of the modulation doping to transfer charge. Most interesting is the fact that, unlike InSb and InGaSb QWs, the mobility of GaSb QWs does not degrade as the density increases over the range studied. As a result, we observe sheet resistivities to drop as low as 1500 Ω/□, a factor of two improvement over the best values for InSb and InGaSb, and much lower than other III–Vs. Our previous results for GaSb QWs on GaAs substrates are not shown on Fig. 7 for clarity, but the lowest resistivity achieved was 3100 Ω/□ [6]. We also include data from the literature for p-InGaAs QWs. The lower mobilities result in resistivities greater than 7000 Ω/□ for InGaAs [27–29].

It is also instructive to compare our p-channel GaSb results to strained Si, currently used for CMOS, and strained Ge, proposed for future CMOS nodes. Fig. 8 includes strained Si data, recent strained Ge data from Intel [30] plus our GaSb data. The GaSb QWs, like Ge QWs, offer substantially higher mobilities and lower sheet resistivities than strained Si. Based upon results from gated hall structures on InGaSb QWs, we expect the GaSb advantage over Si to be maintained at higher carrier densities [31].

Dopants other than Be may be feasible for antimonide p-FET structures. Liao and Cheng investigated carbon doping in InGaSb/AlGaSb QWs [9]. They achieved controllable sheet densities ranging from 0.7 to $4.1 \times 10^{12}/cm^2$. Silicon is an amphoteric dopant in III–V compounds. It is generally n-type for arsenides and InSb, but p-type for GaSb and AlSb [32]. Growth #8 was the same as #4 except that Be was replaced by Si. The resistivity map was very non-uniform, with values ranging from 4100 to 67,000 Ω/□. Transport measurements in the low-resistivity region yielded a mobility of 430 cm^2/V s and a sheet density of $3.4 \times 10^{12}/cm^2$. The results in a more resistive region were: 230 cm^2/V s and $0.8 \times 10^{12}/cm^2$. For growth #9, we changed the dopant layer from AlAsSb to AlSb to avoid electrons from Si dopant atoms in the AlAs. We also rotated the sample during the buffer layer, yielding uniform QW strain

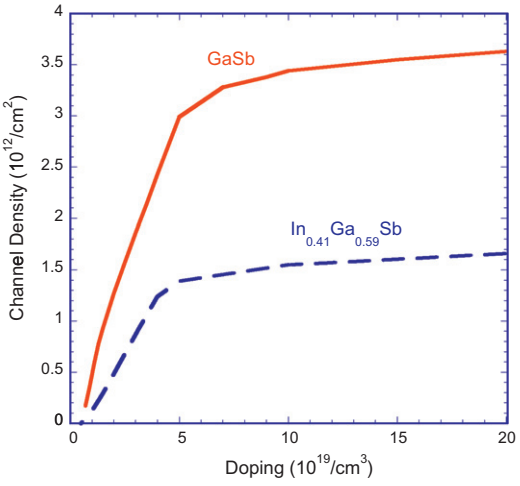

Fig. 9. Calculated hole density in channel as a function of total doping for GaSb and $In_{0.41}Ga_{0.59}Sb$.

across the sample, and did not rotate during the AlSb(Si) layer, yielding a gradient in Si concentration. The resistivity map was again very nonuniform, but all values were above 10,000 Ω/□. For both growths, extremely large anisotropies were observed in the transport measurements, in contrast to the Be-doped samples. It is clear that Si was creating p-type modulation doping in portions of the wafers, but we do not understand the low mobilities or large anisotropies and non-uniformities. In contrast, Be doping in this study and in our previous work on InGaSb- and GaSb-channel pFETs was always well behaved. We reached similar conclusions when comparing Be and Si as dopants for thick layers of AlSb [33].

To investigate the improved high-density performance of GaSb QWs, we have performed additional 8×8 k.p calculations in which we compare GaSb/AlAsSb QW devices with $In_{0.4}Ga_{0.6}Sb$/AlGaSb QW devices. In Fig. 9 we illustrate the effectiveness of doping in the two devices by plotting the channel charge vs. doping concentration for double-sided doping (as in wafer #7) with 5.4 nm spacers and 4 nm doped layers. As the figure shows (and as mentioned

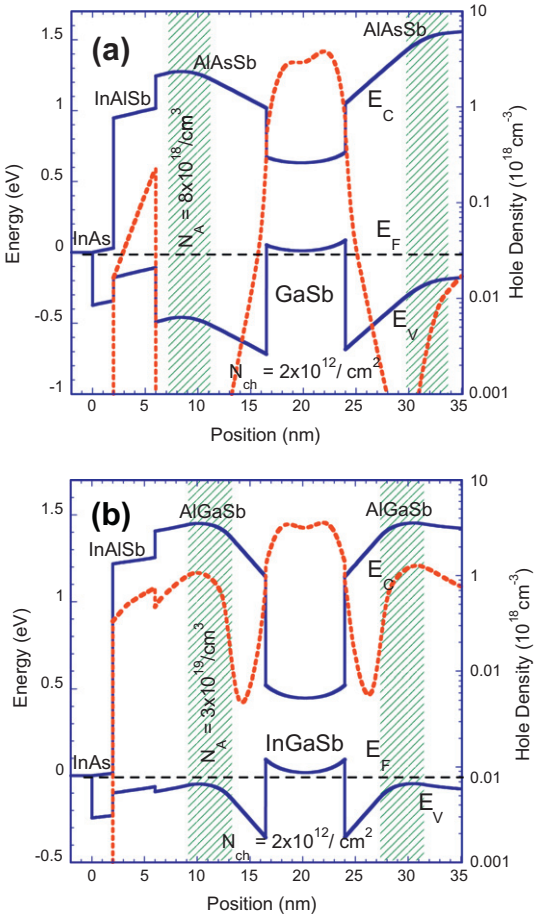

Fig. 10. Calculated band structure and hole density for (a) double-sided doping of a GaSb QW (growth #7) and (b) double-sided doping of $In_{0.41}Ga_{0.59}Sb$. A hole density of $2 \times 10^{12}/cm^2$ is assumed for both heterostructures.

earlier), the larger valence band offset and hence greater well depth of the GaSb QW results in it having a more efficient transfer of charge into the well from the modulation dopant. This explains the saturation of well charge in GaSb at about $3.5 \times 10^{12}/cm^2$ as seen in the experimental data of Fig. 7, although higher values could presumably be reached by decreasing the spacer thickness. In comparison, the saturation level for InGaSb is much lower (unless the dopant is moved closer to the well). The doping efficiency of GaSb is a primary reason why it can reach much lower levels of sheet resistance than InGaSb (or InSb).

A second comparison between GaSb and InGaSb devices is shown in Fig. 10 where we plot their band diagrams and hole density profiles at 300 K. For the devices shown we employ double-sided doping so as to achieve an integrated hole density of $2 \times 10^{12}/cm^2$ in both devices. For the densities considered, the primary subbands occupied are the two highest heavy hole (heavy out-of-plane mass) subbands [6]. Under all these conditions, the lighter in-plane subbands dominate at a sheet density of $2 \times 10^{12}/cm^2$ with the heavier in-plane subbands being separated in energy by 60 meV at −0.5% strain to 260 meV at 3% strain and the occupancy (in the former case) being 2.7%. Again the smaller well depth of the InGaSb QW results in it having a reduced charge transfer efficiency into the well; this is seen in Fig. 10 where to reach the same integrated hole density, the InGaSb device requires that the doping level be both higher ($3 \times 10^{19}/cm^3$ vs. $8 \times 10^{18}/cm^3$ for the GaSb device) and closer to the channel (4 nm vs. 5.4 nm). Also evident in Fig. 10 is the fact that the lower valence band offset and smaller heavy-hole mass of the InGaSb device results in a stronger penetration of the hole wave functions into the barrier (6.4% of the well charge vs. 1.8% for GaSb). Both of these factors – the lower doping and decreased wave function tailing of the GaSb device – will tend to reduce barrier-associated scattering by ionized impurities and/or disorder in the GaSb device as compared to InGaSb. Hence, for a given geometry and well charge, a GaSb device will tend to have a higher mobility and smaller sheet resistance than a comparable InGaSb (or InSb) device as reported in this paper.

4. Conclusions

Quantum wells of GaSb with $AlAs_xSb_{1-x}$ barriers were grown on $AlAs_xSb_{1-x}$ buffer layers on InP substrates as opposed to the GaAs substrates used heretofore. The buffer layer composition was adjusted to yield compressive biaxial strains of 1–3% in the GaSb. The strain-induced modification of the valence band structure, combined with confinement effects, resulted in room-temperature mobilities as high as 1500 cm^2/V s. Similar hole mobilities have been observed in highly strained InSb and InGaSb QWs. For the GaSb wells, however, we found the high mobilities are sustained up to densities of 3.5×10^{12} cm^{-2}. We attribute this enhancement to the GaSb/AlAsSb having the deepest well, and thereby reduced scattering due to stronger confinement and lower levels of doping needed for the same channel charge. The crucial upshot from a device technology perspective is that the sheet resistivity of the GaSb can be as low as 1500 Ω/□, a factor of two lower than any previous III–V p-type QW. GaSb p-channel FETs can thus have lower access resistance and higher drive currents. As such, these high-performance devices together with matching n-channel FETs [34–37] might well serve as the basis for a future ultra-low-power CMOS technology, especially if high-quality gate dielectrics [38] are also incorporated. Of course which material system(s) will win out in the Moore's law endgame is a complicated question that depends on many other factors such as channel hole mobility and velocity, contact resistance, subthreshold slope, I_{on}/I_{off} ratio, and compatibility with n-FET materials [39]. In addition to CMOS, other device technologies may benefit from the advantage of p-GaSb quantum wells with low sheet resistance.

Acknowledgement

The authors thank the Office of Naval Research for funding support.

References

[1] Bennett BR, Magno R, Boos JB, Kruppa W, Ancona MG. Antimonide-based compound semiconductors for electronic devices: a review. Solid State Electron 2005;49:1875–95.
[2] Chau R, Datta S, Doczy M, Doyle B, Jin J, Kavalieros J, et al. Benchmarking nanotechnology for high-performance and low-power logic transistor applications. IEEE Trans Nanotechnol 2005;4:153–8.
[3] Ruden PP, Shur M, Arch DK, Daniels RR, Grider DE, Nohava TE. Quantum-well p-channel AlGaAs/InGaAs/GaAs heterostructure insulated-gate field-effect transistors. IEEE Trans Electron Dev 1989;36:2371–9.
[4] Bennett BR, Ancona MG, Boos JB. Compound semiconductors for low-power p-channel field-effect transistors. MRS Bull 2009;34:530–6.
[5] Oktyabrsky S. p-Type channel field-effect transistors. Fundamentals of III–V semiconductor MOSFETs; 2010. p. 349-78
[6] Bennett BR, Ancona MG, Boos JB, Canedy CB, Khan SA. Strained GaSb/AlAsSb quantum wells for p-channel field-effect transistors. J Cryst Growth 2008;311:47–53.
[7] Bennett BR, Ancona MG, Brad Boos J, Shanabrook BV. Mobility enhancement in strained p-InGaSb quantum wells. Appl Phys Lett 2007;91:042104.
[8] Klem JF, Lott JA, Schirber JE, Kurtz SR, Lin SY. Strained quantum-well modulation-doped InGaSb/AlGaSb structures grown by molecular-beam epitaxy. J Electron Mater 1993;22:315–21.

[9] Liao C, Cheng KY. Hole mobility in pseudomorphic InGaSb quantum well modulation doped with carbon. J Vac Sci Technol B 2010:28.
[10] Radosavljevic M, Ashley T, Andreev A, Coomber SD, Dewey G, Emeny MT, et al. High-performance 40 nm gate length InSb p-channel compressively strained quantum well field effect transistors for low-power (VCC = 0.5 V) logic applications. In: IEEE international electron devices meeting. Technical digest; 2008. p. 727–30.
[11] Tokranov V, Nagaiah P, Yakimov M, Matyi RJ, Oktyabrsky S. AlGaAsSb superlattice buffer layer for p-channel GaSb quantum well on GaAs substrate. J Cryst Growth 2011;323:35–8.
[12] Gaspe CK, Edirisooriya M, Mishima TD, Jayathilaka PARD, Doezema RE, Murphy SQ, et al. Effect of strain and confinement on the effective mass of holes in InSb quantum wells. J Vac Sci Technol B 2011:29.
[13] Boos JB, Bennett BR, Papanicolaou NA, Ancona MG, Champlain JG, Chou YC, et al. Sb-based n- and p-channel heterostructure FETs for high-speed, low-power applications. IEICE Trans Electron 2008;E91C:1050–7.
[14] Takei K, Madsen M, Fang H, Kapadia R, Chuang S, Kim HS, et al. Nanoscale InGaSb heterostructure membranes on Si substrates for high hole mobility transistors. Nano Lett 2012;12:2060–6.
[15] Boos JB, Bennett BR, Papanicolaou NA, Ancona MG, Champlain JG, Park D, et al. In: Device research conference; 2009. p. 159–62.
[16] Canedy CL, Boishin GI, Bewley WW, Kim CS, Vurgaftman I, Kim M, et al. Correlating growth conditions with photoluminescence and lasing properties of mid-IR antimonide type II "W" structures. J Vac Sci Technol B 2004;22:1575–9.
[17] Zhang YH. Accurate control of As and Sb incorporation ratio during solid-source molecular-beam epitaxy. J Cryst Growth 1995;150:838–43.
[18] Passlack M, Droopad R, Rajagopalan K, Abrokwah J, Gregory R, Nguyen D. High mobility nMOSFET structure with high-k-dielectric. IEEE Electron Device Lett 2005;26:713–5.
[19] Bennett BR, Tinkham BP, Boos JB, Lange MD, Tsai R. Materials growth for InAs high electron mobility transistors and circuits. J Vac Sci Technol B 2004;22:688–94.
[20] Lange MD, Tsai RS, Deal WR, Nam PS, Lee LJ, Sandhu RS, et al. InAs/AlSb high-electron-mobility transistors by molecular-beam epitaxy for low-power applications. J Vac Sci Technol B 2006;24:2581–5.
[21] Luo LF, Longenbach KF, Wang WI. Para-channel modulation-doped field-effect transistors based on AlSbAs/GaSb. IEEE Electron Dev Lett 1990;11:567–9.
[22] Yoh K, Taniguchi H, Kiyomi K, Inoue M. Complementary InAs n-channel and GaSb p-channel quantum-well heterojunction field-effect transistors. Jpn J Appl Phys 1991;30:3833–6.
[23] Birner S, Zibold T, Andlauer T, Kubis T, Sabathil M, Trellakis A, et al. Nextnano: general purpose 3-D simulations. IEEE Trans Electron Dev 2007;54:2137–42.
[24] Klem JF, Fu WS, Gourley PL, Jones ED, Brennan TM, Lott JA. Role of substrate threading dislocation density in relaxation of highly strained InGaAs/GaAs quantum-well structures. Appl Phys Lett 1990;56:1350–2.
[25] Meshkinpour M, Goorsky MS, Jenichen B, Streit DC, Block TR. The role of substrate quality on misfit dislocation formation in pseudomorphic high electron mobility transistor structures. J Appl Phys 1997;81:3124–8.
[26] Bennett BR. Strain relaxation in InAs/GaSb heterostructures. Appl Phys Lett 1998;73:3736–8.
[27] Kusters AM, Kohl A, Sommer V, Muller R, Heime K. Optimized double-heterojunction pseudomorphic InP/InGaAs/InP p-MODFETs and the role of strain in their design. IEEE Trans Electron Dev 1993;40:2164–70.
[28] Nagaiah P, Tokranov V, Yakimov M, Oktyabrsky S. Strained quantum wells for p-channel InGaAs CMOS. Perform Reliab Semicond Dev 2009;1108:231–6.
[29] Park H, Mandeville P, Saito R, Tasker PJ, Schaff WJ, Eastman LF. RF and DC characterization of para-channel AlGaAs/GaAs MODFETs with gate length as small as 0.25 microns. In: Proceedings: IEEE/Cornell conference on advanced concepts in high speed semiconductor devices and circuits; 1989. p. 101–10.
[30] Pillarisetty R, Chu-Kung B, Corcoran S, Dewey G, Kavalieros J, Kennel H, et al. High mobility strained germanium quantum well field effect transistor as the p-channel device option for low power (Vcc=0.5 V) III–V CMOS Architecture. In: International electron devices meeting 2010. Technical Digest; 2010.
[31] Nainani A, Bennett BR, Boos JB, Ancona MG, Saraswat KC. Enhancing hole mobility in III–V semiconductors. J Appl Phys 2012;111:103706.
[32] Venkatasubramanian R, Dorsey DL, Mahalingam K. Heuristic rules for group IV dopant site selection in III–V compounds. J Cryst Growth 1997;175:224–8.
[33] Bennett BR, Moore WJ, Yang MJ, Shanabrook BV. Transport properties of Be- and Si-doped AlSb. J Appl Phys 2000;87:7876–9.
[34] Bennett BR, Ancona MG, Champlain JG, Papanicolaou NA, Boos JB. Demonstration of high-mobility electron and hole transport in a single InGaSb well for complementary circuits. J Cryst Growth 2009;312:37–40.
[35] Ali A, Madan H, Agrawal A, Ramirez I, Misra R, Boos JB, et al. Enhancement-mode antimonide quantum-well MOSFETs with high electron mobility and gigahertz small-signal switching performance. IEEE Electron Dev Lett 2011;32:1689–91.
[36] Desplanque L, Vignaud D, Godey S, Cadio E, Plissard S, Wallart X, et al. Electronic properties of the high electron mobility $Al_{0.56}In_{0.44}Sb/Ga_{0.5}In_{0.5}Sb$ heterostructure. J Appl Phys 2010;108:043704.
[37] Loesch R, Aidam R, Kirste L, Leuther A. Molecular beam epitaxial growth of metamorphic AlInSb/GaInSb high-electron-mobility-transistor structures on GaAs substrates for low power and high frequency applications. J Appl Phys 2011;109:033706.
[38] Nainani A, Irisawa T, Yuan Z, Bennett BR, Boos JB, Nishi Y, et al. Optimization of the Al_2O_3/GaSb interface and a high-mobility GaSb pMOSFET. IEEE Trans Electron Dev 2011;58:3407–15.
[39] Ancona MG, Bennett BR, Boos JB. Scaling projections for Sb-based p-channel FETs. Solid State Electron 2010;54:1349–58.